High Rate Li-Ion Storage Property of MOFs-Carbonized Derivatives Coating on MnO Nanowires

Zhen-Dong Huang [a], [†] Zhen Gong [a], [†] Qi Kang [a], Yanwu Fang [a], Xu-Sheng Yang [b], Ruiqing Liu [a], Xiujing Lin [a], Xiaomiao Feng [a], Yanwen Ma [a],* and Dan Wang [a, c],*

Recently, metal-organic frameworks (MOFs) derived porous carbon-based composites have become one of the advanced electrode materials for high performance energy storage systems. In this work, zeolitic imidazolate framework (ZIF) type of MOFs strung by MnO_2 NWs, forming an interesting structure like Chinese candied hawthorn fruit on a stick, are used as precursor to prepare C/Co-coating MnO nanowires (C/Co-MnO NWs). It is interesting and exciting to observe that the simultaneously formed carbon coating derived from ZIFs significantly promote the cyclic and rate performance of manganese oxide because of the synergistic effect of the highly conductive uniform carbon coating and the high capacity contribution from MnO NWs. The obtained C/Co-MnO NWs could deliver 848.4 and 718 $mAhg^{-1}$ at 500 and 5000 mAg^{-1} after 40 charge/discharge cycles, respectively, which are superior to other reported MOF-derived nanostructured materials, and make it to be a very promising candidate anode materials for future high-power lithium ion batteries.

Introduction

A worldwide recognition for the importance of green energy storage and distribution to people's daily life and atmospheric environment have been received now with urban environment decay. The incomplete combustion of fossil fuel to power traditional vehicle and to supply the heat for space heating is considered as one of the main reasons responsible for the more and more serious fog and haze condition in large city, especially in developing countries. Therefore, the ever-increasing demand on the electrical vehicle (EV) and low cost green energy harvest station is accelerating the development of advanced energy storage and energy conversion systems. Currently, lithium-ion batteries (LIBs) are leading the power sources market for EV and still predominate the battery market for portable electronic devices and green energy distribution because of their high energy density, long life span, no memory effect, and environmental benignity. [1-3] However, the traditional LIBs using graphite as anode material are not able to satisfy the rapidly expanding demand due to the limited theoretical capacity of graphite (372 mA h g^{-1}). [2-6] Thus, one of the urgent research interests for materials scientists delved into next generation energy storage technology is to develop a novel low cost anode materials with higher capacity and better cycle stability at higher power state.

Nowadays, other than various advanced carbon material, nanostructured silicon-based hybrids, nanostructured transition metal and their oxides or sulfides have attracted intensive interesting because of their much higher theoretical lithium ion storage capacity. [5-16] However, the semi-conductive or even insulating nature and huge volume change during the (de)lithiation process are two of their intrinsic drawbacks as anode materials for LIBs. Hereinto, Mn-based oxides, such as MnO, MnO_2 and Mn_3O_4, [16-25] have been extensively studied as promising candidate anode materials due to their relatively smaller volume change than Si and their environmental benign nature. However, the same as other transitional metal oxide anode materials for LIBs, the rate capability and cyclic stability of Mn-based oxide anodes also have to be solved before practical application. As for the less conductive Mn-based oxides, the significant volume change during the charge-discharge process again will lead to the pulverization of active particles and their detaching from conductive network or current collector, in turn to finally increase system charge transfer resistance and reduce the availability of active substance.

In recent years, great efforts have been made by material scientists to solve the aforementioned problems encountered by Mn-based oxide anodes. For example, binary manganese oxides ($M_xMn_yO_z$) have been developed as promising anode candidates with enhanced electrochemical performance, [20] since most of the research results indicate that binary metal

[a] *Key Laboratory for Organic Electronics and Information Displays & Institute of Advanced Materials (IAM), Jiangsu National Synergetic Innovation Center for Advanced Materials (SICAM), Nanjing University of Posts & Telecommunications, Nanjing 210023, China.*

[b] *Advanced Manufacturing Technology Research Centre, Department of Industrial and Systems Engineering, The Hong Kong Polytechnic University, Hung Hom, Kowloon, Hong Kong, China.*

[c] *State Key Laboratory of Multiphase Complex Systems Institute of Process Engineering Chinese Academy of Sciences, No. 1, Beiertiao, Zhongguancun, Beijing, 100190, P.R. China.*

† Dr. Huang and Mr. Gong have the equal contribution to this paper.

* Corresponding authors:

iamywma@njupt.edu.cn (Y.W. Ma); danwang@ipe.ac.cn (D Wang)

Electronic Supplementary Information (ESI) available: [details of any supplementary information available should be included here]. See DOI: 10.1039/x0xx00000x

oxides exhibit better conductivity and structure stability than that of mono metal oxides. Development of nanostructured hierarchical Mn-based oxides is also one of the important strategies to promote the cyclic and rate capability of Mn-based anode materials. [16] Furthermore, constructing uniform 3 dimensional conductive network via introduction of uniform surface coating and formation of nanostructured composite with carbon is considered as one of the most important and effective way to achieve superior rate and cyclic stability of Mn-based oxide anode materials. [1 7-21] The introduction of carbon materials, such as carbon nanotube, graphene and nitrogen-doped carbon coating, not only can help to accelerate charge transport, but also is helpful for the formation of stable solid electrolyte interphase and the remission of inner stress caused by the huge volume change.

In last few years, metal-organic frameworks (MOFs), constructed with metal ions or clusters and poly functional organic ligands, have attracted increasing attention from both fundamental scientific research and practical multifunctional applications in these years. [9-29] Zeolitic imidazolate frameworks (ZIFs) type of MOFs, such as ZIF-67, ZIF-8, [9-14] are high porosity and considered as one of the MOFs promising for commercial applications. Especially, the carbonized derivatives of ZIFs showed good potential application in LIBs. For instance, the ZIF nanocrystals derived carbon anode material showed a good cyclic stability and a superior rate capability. [27-29] However, the very low tap density of the highly porous nanostructure, together with the relatively low capacity, limited their practicability as anode materials for commercial LIBs. Nevertheless, the unique structure and composition of ZIFs and their carbonized derivatives are very helpful to design different nanostructure transition metal and their oxides and to improve their rate and cyclic stability.

Based on above concerns, an interesting structure of MOFs ZIF-67 on MnO_2 nanowire (NWs) is designed and prepared by using a controllable way in this work, as inspired by the interesting structure of the candied hawthorn fruit on a stick. Furthermore, the simultaneously formed carbon coating derived from ZIF-67 is designed to promote the cyclic and rate performance of manganese oxide. Benefited from the synergistic effect of the highly conductive uniform carbon coating and the high capacity contribution from MnO, the finally obtained C/Co-MnO NWs composites shows a high reversible capacity of 848.4, 836.5, 834 and 718 mA h g^{-1} at 500, 1000, 2000 and 5000 mA g^{-1} after 40 charge/discharge cycles, respectively.

Experimental

Materials and Synthetic procedures

General procedure for synthesis of MnO_2 NWs. The MnO_2 NWs were synthesized by a graphene oxide (GO) modified hydrothermal method referred to [30]. The typical processes are as follows: Initially, the GO powder, as-prepared by following our modified Hummers' method, [8] was dispersed into ultra-pure water to get a 2 mg mL^{-1} GO aqueous solution. Subsequently, 0.35 g of manganese sulfate monohydrate ($MnSO_4 \cdot H_2O$, Guangdong Xilong Chemical) was dissolved into 7.5 mL GO aqueous solution to form a clear solution, labeled as solution A. Meanwhile, 0.5g potassium permanganate ($KMnO_4$, Shanghai Lingfeng Chemical) was dissolved into 10 mL distilled water to get a clear solution B. Subsequently, the solution B was dropwisely added into the solution A under magnetic stirring. By following the reaction below:

$2KMnO_4 + 3MnSO_4 + 2H_2O \rightarrow 5MnO_2 + K_2SO_4 + 2H_2SO_4$

A dark brown precipitate gradually appeared with the oxidation of Mn^{2+} precursor by the strong oxidizer. After 15 mins ultrasonication treatment, the obtained brown dispersion was sealed into a 50 mL Teflon-lined stainless steel autoclave and put into a blowing drying box preheated to 140 ^{o}C. After 2h hydrothermal reaction, the solid product were collected and washed several times with distilled water and ethyl alcohol through centrifugate. Being dried at 60 °C for 24 h in vacuum drying oven, the MnO_2 NWs was finally obtained and kept for next step.

Controllable self-assembly process for the unique structure of ZIF-67 on MnO_2 NWs. The typical self-assembly process for the unique structure of ZIF-67 on MnO_2 NWs (ZIF-67-MnO_2 NWs) is as follows: At the beginning, 30 mg nanowires were uniformly dispersed into 20 mL of methanol with the aid of ultrasonication. Then, 100 mg polyvinylpyrrolidone (PVP, Shanghai Aladin Ltd) was dissolved into MnO_2 NWs dispersions to modify the surface of NWs. Subsequently, 100 mg cobalt nitrate hexahydrate ($Co(NO_3)_2 \cdot 6H_2O$, Wuxi Yasheng Chemical) was added into above solution, marked as solution A; At last, 10 ml solution B (0.2 g mL^{-1} 2-methylimidazole (Shanghai Aladin Ltd) in methanol) was mixed into solution A drop by drop. Being settled for 24 h, purple solid product was collected by centrifugation, washed with methanol three times. After drying at 60 °C for 24 h in vacuum drying oven, the final product of ZIF-67-MnO_2 NWs was obtained and kept for the next step. The controlled ZIF-67-MnO_2 NWs mixture was prepared by the same process mentioned above without using PVP. The controlled ZIF-67 pure MOFs were prepared by the same process mentioned above without using PVP and MnO_2 NWs.

Preparation of the carbonized derivatives from ZIF-67 and ZIF-67 on MnO_2 NWs. In order to obtain the finally carbon derivatives, the as-prepared ZIF-67 and ZIF-67 on MnO_2 NWs were carbonized at 300 and 550 °C for 3 h with a temperate ramp of 1 °C min^{-1} under N_2 atmosphere in a horizontal tube furnace, respectively. Being naturally cooled to room temperature, the black reminders, namely C/Co and C/Co-MnO NWs, were finally obtained as anode materials for LIBs. As for comparison, the controlled mixture of MnO_2 NWs and Co/C derivatives was also prepared by physically mixing the as-prepared MnO_2 NWs (75wt%) and Carbonized ZIF-67 (25wt%) via ultrasonication in ethanol, followed by drying the dispersion at 60 ^{o}C for 10 h in blowing drying oven.

Characterization

The morphology of MnO_2 NWs, ZIF-67, ZIF-67-MnO_2 NWs, C/Co and C/Co-MnO NWs were characterized by using field emission scanning electron microscopy (FE-SEM, Hitachi S-4800) at an acceleration voltage of 3 kV and field emission transmission electron microscope (FE-TEM, JEOL 2010F) at an accelerating voltage of 200 kV. Nitrogen adsorption/desorption isotherms were gained at 77 K using an automated adsorption apparatus (Micromerit-ics ASAP2020). The surface area was calculated based on the Brunauer–Emmett–Teller (BET) equation. The X-ray diffraction patterns of MnO_2 NWs, ZIF-67,

ZIF-67-MnO_2 NWs, C/Co and C/Co-MnO NWs were measured on an X-ray diffractometer (RIGAKU, RINT-ULTIMA III) using Cu Kα radiation (λ=1.54051 Å). The diffraction patterns were recorded in the 2θ range of 5 – 75° with a step size of 0.01 °. The elemental mapping of C/Co-MnO NWs was characterized by energy-dispersive X-ray spectroscopy (EDS, Oxford instruments X-Max). The content of Co and Mn within as-prepared C/Co-MnO NWs was measured by following the general rules JY/T 015-1996 for inductively coupled plasma-atomic emission spectrometry (ICP-AES, Prodigy, Teledyne Leeman Labs).

To investigate the electrochemical performances, the as-prepared active materials, including MnO_2 NWs, ZIF-67, ZIF-67-MnO_2 NWs, C/Co and C/Co-MnO NWs, were homogeneously mixed with conductive additive (acetylene black) and binder (PVDF) in a weight ratio of 75% / 15% / 10% in a proper amount of N-methylpyrrolidinone solvent to form a uniform slurry. The working electrodes were prepared by coating the obtained slurry on copper foil which was acted as a current collector. The electrode was then punched out into 10 mm (in diameter) disks. The average mass loading of active materials is about 1.27 $mgcm^{-2}$.Two-electrode lithium ion batteries were assembled in an ultrapure Ar-gas filled glove box to investigate the lithium ion storage performance of MnO_2 NWs, ZIF-67, ZIF-67-MnO_2 NWs, C/Co and C/Co-MnO NWs. The electrolyte used was a 1 mol L^{-1} $LiPF_6$ in ethylene carbonate (EC) + dimethyl carbonate (DMC) + ethyl methyl carbonate (EMC) in a volume ratio of 1:1:1. Lithium discs were used as counter electrodes. Cyclic voltammetry (CV) and galvanostatic charge and discharge measurements were carried out in a voltage range of 0.01 to 3 V vs Li/Li^+ at a current density ranging from 0.5 to 5 A g^{-1}, respectively. The electrochemical impedance spectroscopy was carried out in a frequency range of 0.01 Hz to 100 kHz, and the perturbation amplitude was controlled at 5 mV. The galvanostatic charge/discharge test were performed on a battery testing system (CT2001A, Wuhan Land).

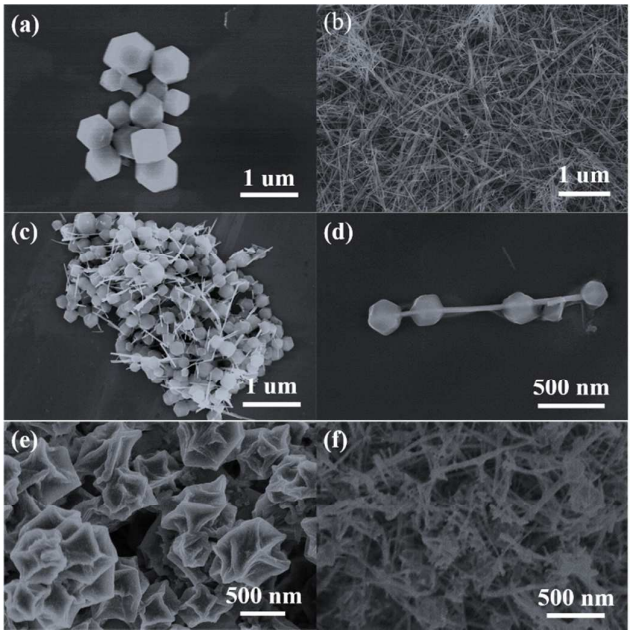

Fig. 1. Scanning electron microscopy (SEM) images of as-prepared (a) ZIF-67, (b) MnO_2 NWs, (c) and (d) ZIF-67-MnO_2 NWs, (e) carbonized derivative of ZIF-67 (C/Co) and (f) carbonized derivative of ZIF-67-MnO_2 NWs (C/Co-MnO NWs), respectively.

Results and discussions

Morphology and structure

ZIF-67. In this work, one type of ZIF series MOFs, namely ZIF-67, was successfully prepared as a control electrode materials and the important building block for the nanostructure of MOF on MnO_2 NWs. The typical polyhedron morphology of the controlled ZIF-67 shown in Fig. 1a is similar with the reported work. [31] The obtained ZIF-67 polyhedrons have a narrow particle size ranged from 500 ~ 800 nm. The X-ray diffraction pattern, shown in Fig. 2a (red), is matched well with that of reported structure of ZIF-67. [31] The nitrogen adsorption/desorption isotherm and pore-size distribution curves in red presented in Figs. 2c and 2d indicates the microporous characteristics of ZIF-67 with a BET specific surface area of 1158.4 $m^2 g^{-1}$. This observation is also similar with other reported works.

MnO_2 NWs. The same as ZIF-67, the MnO_2 NWs were also prepared as the important building block for the nanostructure of MOF on MnO_2 NWs. With the modification of GO, the MnO_2 NWs prepared through the modified hydrothermal reaction have a large ratio of length to diameter. The length is about 2 ~ 3 μm, seeing Fig.1b, while the diameter is around 10 ~ 30 nm, as shown in Fig. 3d. Its BET specific surface area of 77.327 $m^2 g^{-1}$, obtained from the nitrogen adsorption/desorption isotherm shown in Fig. 2c (black), further reflects the nanoscale nature of the product. The X-ray diffraction pattern given in Fig. 2a (black) indicates that the obtained NWs is potassium doped MnO_2, $K_{2-x}Mn_8O_{16}$ (PDF#44-1386), which belongs to the monoclinic I2/m (12) space group. The high resolution TEM images and the composition analysis result provided in Figs. 3e, 3f and 4d further confirm the observed structure and composition of the obtained MnO_2 NWs. The measured lattice fringes (Figs. 3e and 3f) with an interplane distances of 0.314, 0.2772 and 0.1847 nm can be indexed to the (30-1), (110) and (41-1) crystallographic plane of the monoclinic $K_{2-x}Mn_8O_{16}$ structure, respectively.

ZIF-67-MnO_2 NWs. With the aim to exploit the advantage of both MOF and manganese oxide NWs, a unique structure of MOFs on NWs have been designed and successfully developed in this work. During the preparation process, PVP was used to modify the surface condition of MnO_2 NWs. With the help of surface modification, MOFs ZIF-67 was uniformly grown on the surface of MnO_2 NWs. Although the developed structure of Chinese candied hawthorn fruit on a stick of the ZIF-67 on MnO_2 nanowire (ZIF-67-MnO_2 NWs) is similar with previously reported work, [32] the designing mentality, the preparation process and the final products in this work are different from the research work done in [32]. As shown in Figs. 1c, 1d and 3d, MnO_2 NWs strung all ZIF-67 polyhedron to form a unique structure like that of Chinese candied hawthorn fruit on a stick or pearl necklace and lamb skewer. Interestingly, the ZIF-67 polyhedrons on MnO_2 NWs are only about 100 nm, which is much smaller than of pure ZIF-67 polyhedrons (500 ~ 800 nm) grown in the same process and the reported ZIF-67 on MnO_2 NW prepared with aid of polyetherimide (PEI). [32] It is also valuable to note that the sample prepared without using PVP is the mixture of ZIF-67 and MnO_2 NWs, as shown in Fig. S1a. Although the size of obtained ZIF-67 particles are also slightly reduced to 300 ~ 400 nm, still larger

than that of ZIF-67-MnO_2 NWs. The results mentioned above vigorously indicate that the obviously heterogeneous nucleation phenomenon on the PVP modified surface of MnO_2 NWs should be responsible for the uniform growth

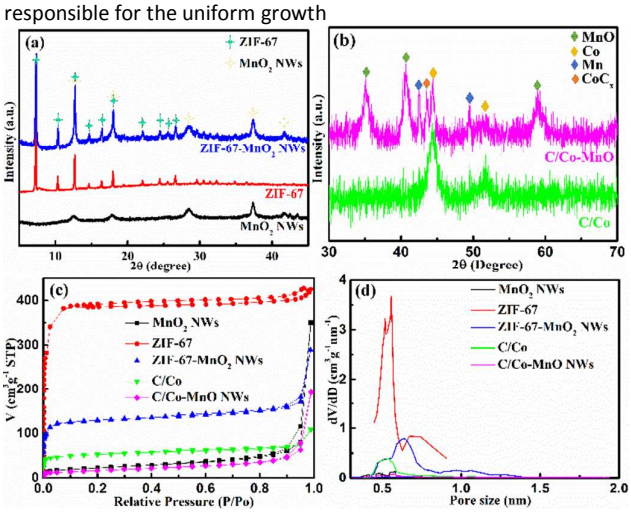

Fig. 2. (a), (b) X-ray diffraction (XRD) patterns, (c) nitrogen adsorption/desorption isotherm profile and (d) pore-size distribution curves of as-prepared MnO_2 NWs (in black), ZIF-67 (in red), ZIF-67-MnO_2 NWs (in blue), carbonized derivative of ZIF-67 (C/Co) (in green) and carbonized derivative of ZIF-67-MnO_2 NWs (C/Co-MnO NWs) (in pink), respectively.

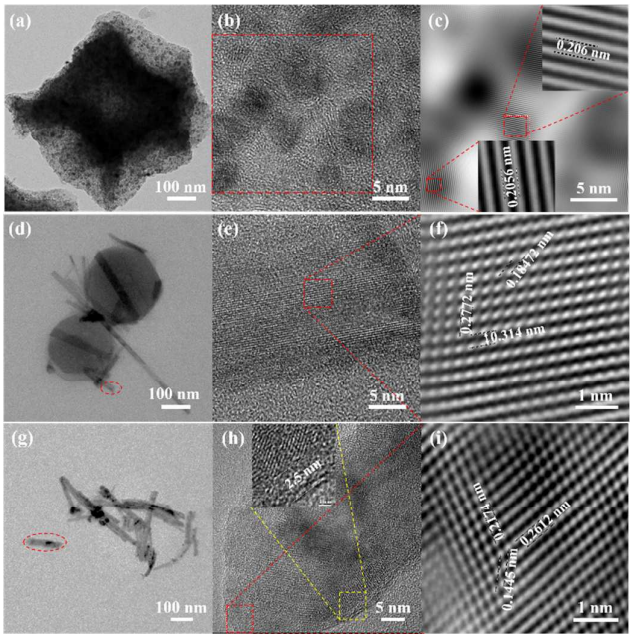

Fig. 3. High resolution transmission electron microscopy (HR-TEM) images of as-prepared carbonized derivative of ZIF-67 (C/Co) (a, b and c), ZIF-67-MnO_2 NWs (d, e and f), and carbonized derivative of ZIF-67-MnO_2 NWs (C/Co-MnO NWs) (g, h and i), respectively.

of the much smaller particle size of ZIF-67 polyhedrons on MnO_2 NWs. The X-ray diffraction pattern present in Fig. 2a is the combined patterns of both ZIF-67 and MnO_2, which further confirms the successful growth of the unique structure of MOFs ZIF-67 on MnO_2 NWs (ZIF-67-MnO_2 NWs). The large BET specific surface area (520.975 $m^2 g^{-1}$) and the microporous structure, observed from Figs. 2c and 2d, further indicate that the as-prepared ZIF-67-MnO_2 NWs maintain the advantages nature of ZIF-67.

C/Co and C/Co-MnO NWs. In order to obtain highly conductive materials for high rate LIBs, both ZIF-67 and ZIF-67-MnO_2 NWs were carbonized at a temperature of 550 °C for 3 h under Ar gas atmosphere. As shown in Fig.1e, the ZIF-67 polyhedrons became withered, like Chinese traditional wonton. The XRD diffraction pattern and the high resolution TEM image shown in Figs. 2b, 3a, 3b and 3c, respectively, indicate that the carbonized derivative of ZIF-67 is the composite of carbon and cobalt nanoparticles (C/Co). As indexed by the high resolution TEM image shown in Figs. 3b and 3c, The measured lattice fringes with an interplane distance of 0.206 nm can be indexed to the (111) crystallographic plane of the cubic cobalt, belonged to the crystal space group of Fm-3m (225). This observation indicate that the cobalt component within ZIF-67 are reduced to elemental metallic cobalt nanoparticle after a carbothermic reduction reaction. Furthermore, the cubic metallic cobalt particles, dispersed into the carbon matrix, are about 2~5 nm. During the carbonization process, the structure became dense. As shown in Figs. 2c and 2d, the specific surface area and the pore volume decrease from 1158.4 $m^2 g^{-1}$ and 0.66 $cm^3 g^{-1}$ of ZIF-67 to 193.755 $m^2 g^{-1}$ and 0.078 $cm^3 g^{-1}$ of C/Co composites, respectively. Similar with the obtained C/Co composites, the carbonized derivative of ZIF-67-MnO_2 NWs becomes the complex composites of carbon, cobalt nanoparticles and MnO NWs (C/Co-MnO NWs) with little amount of Mn and CoC_x formed during the carbonization process, as indicated by the pink color X-ray diffraction pattern shown in Fig. 2b. As shown in Fig S1b, the morphology of ZIF-67 on MnO_2 NWs still maintain after 3 h annealing at 300 °C. However, Being calcined at 550 °C for 3 h, ZIF-67 polyhedrons have been molten and formed a uniform carbon coating on the surface of MnO NWs reduced from MnO_2 NWs, which can be observed from the SEM image shown in Fig. 1f and the high resolution TEM images present in Figs. 3g, 3h and 3i, and further confirmed by the elements mapping results demonstrated in Fig. S2. The measured lattice fringes (Figs. 3h and 3i) with an interplane distances of 0.2612, 0.2174 and 0.1445 nm can be indexed to the (111), (200) and (311) crystallographic plane of the cubic MnO structure in the space group of Fm-3m (225), respectively. The uniform carbon coating, about 2~3 nm in thickness, can be observed from the inset of Fig. 3h, which is good for the construction of 3D conductive network. As for Mn and CoCx impurity phase, it is very difficult to define them from the high resolution TEM images together with MnO, due to their small amount and similar interlayer space. Based on the distribution of Co shown in Fig. S2c, cobalt mainly gather on the location of polyhedron sites. The ICP-AES measurement result indicates the element content of Co and Mn within the finally obtained C/Co-MnO NWs are about 16.0% and 43.8%, respectively. The nitrogen adsorption/desorption isotherm and pore-size distribution curves presented in Figs. 2c and 2d confirm that the BET specific surface area of C/Co-MnO NWs further decreased to 57.8 $m^2 g^{-1}$, which would be good to obtain higher volumetric energy density.

Lithium ion storage properties

In this work, the galvanostatic charge/discharge measurements at different current density, the cyclic voltammetry (CV) and electrochemical impedance spectroscopy (EIS) were carried out in lithium half-cells to investigate and to understand the electrochemical behaviour of as-prepared active materials. Fig. 4 and Fig. 5 indicate that MnO_2 NWs, ZIF-67-MnO_2 NWs, C/Co, and C/Co-MnO NWs are electrochemical active, and capable of lithium ion storage. As shown in Fig. 4a, the typical CV curves of the second cycle scanning between 0.01 and 3.0 V at 0.1 mV s^{-1}, which is similar with the reported MnO/C materials, [17, 18] demonstrate that the electrode made of C/Co and C/Co-MnO NWs show smaller voltage gap between reduction and oxidation peaks, meanwhile, the CV curve of C/Co-MnO NWs shows larger peak current density than that of C/Co resulted from the higher fraction of high capacity transition metal components. A pair of weak typical redox peaks could be found from the CV curve of C/Co shown in Fig. 4a, which indicates that Co have a relatively minor contribution to the capacity of C/Co electrode. Therefore, the CV analysis result clarify that C/Co-MnO NWs shows better electrochemical performance due to the synergistic effect of MnO NWs and its uniform MOF derived carbon coating. It can be found from Fig. 4b that C/Co and C/Co-MnO NWs shows much lower charge transfer resistance than that of MnO_2 NWs and ZIF-67-MnO_2 NWs. After fitting with the equivalent circuit shown in the inset of Fig. S3c, the calculated resistances, including the electrolyte resistance and the contact resistance of the active materials to current collector, is around 4.2 Ω. The charge transfer resistance (R_{ct}), equal to the diameter of the semicircle in the high frequency range, is about 65.9 Ω.

Furthermore, in the Bode plots given in Fig. S3d, the characteristic frequencies f_0 at the phase angle of -45 ^{o} for C/Co-MnO NWs, C/Co, ZIF-67-MnO_2 NWs, and MnO_2 NWs are 0.071 , 0.067, 0.026 and 0.010 Hz, corresponding to the time constant τ_0 (τ_0=1/ f_0) of 14.1, 14.9, 38.5 and 100 s, respectively. The value of C/Co-MnO NWs are greatly smaller than those of the materials mentioned earlier, indicating the fast charge-discharge rate of the C/Co-MnO NWs than others. This observation further reflects that the improved conductivity of C/Co-MnO NWs, sprung from the uniform carbon coating on MnO NWs, are responsible to its better electrochemical performance.

The typical charge/discharge profiles present in Fig. S3, Fig. 4c and Fig. 4d for the first cycle and the 40th cycle, respectively, also evidently prove that the electrode made of C/Co-MnO NWs delivers much higher capacity with an excellent rate capability than other electrodes prepared with other controlled materials. The Li//C/Co-MnO NWs half-cell exhibits much higher capacity, higher columbic efficiency for the first cycle and better cyclic performance than that of Li//MnO_2 NWs half-cell, which should be promoted by the ZIF-67-derived surface layer of C/Co. With respect to ZIF-67-derived C/Co, a typical discharge plateau and reduction peak obviously observed at the voltage of 0.5 V should be resulted from the reduction of Mn^{2+} to Mn^0. The corresponding redox reaction of Mn^{2+}/Mn^0 should be accounted for the higher capacity of C/Co-MnO NWs over C/Co. This lithium ion storage mechanism is similar with other reported MnO@C composites. [17, 33] Moreover, the synergistic effect of MnO NWs and its uniform MOF derived carbon coating should be responsible to the superior lithium ion storage performance, compared to ZIF-67-MnO_2 NWs. This results is consistent with the CV analysis results, see Figs. 4a and 4c. As shown in Fig.4d, the specific charge capacity of C/Co-MnO NWs are 848.4, 836.5, 834 and 718 mA h g^{-1} at 500, 1000, 2000 and 5000 mA g^{-1} after 40 charge/discharge cycles, respectively, which confirm the superior rate capability of the as-prepared C/Co-MnO NWs. Figs.5 and Fig. S4 further exhibits that the as-prepared C/Co-MnO NWs not only delivered much better rate

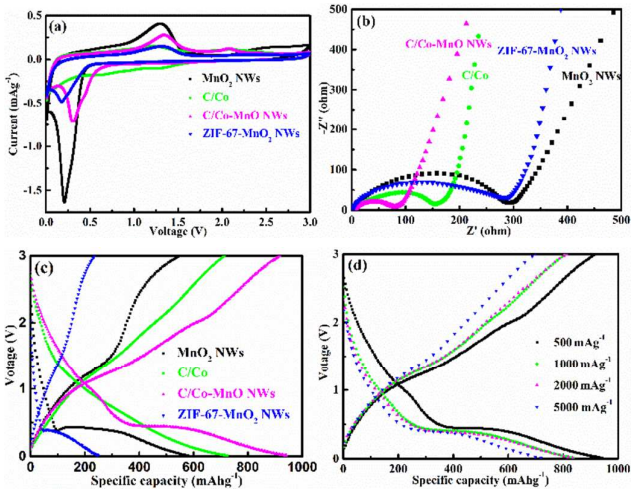

Fig. 4. (a) cyclic voltammetry (CV) curves, (b) electrochemical impedance spectroscopies, (c) the charge/discharge profile at 40th cycle of as-prepared MnO_2 NWs (in black), ZIF-67-MnO_2 NWs (in blue), carbonized derivative of ZIF-67 (C/Co) (in green) and carbonized derivative of ZIF-67-MnO_2 NWs (C/Co-MnO NWs) (in pink), respectively, and (d) the charge/discharge profile at 40th cycle of C/Co-MnO NWs at the current density from 500 to 5000 mAg^{-1}.

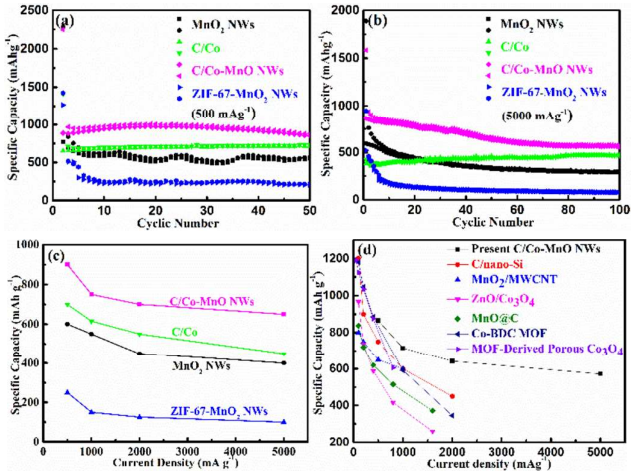

Fig. 5. (a) and (b) the cyclic performance of C/Co-MnO NWs at the current density of 500 and 5000 mAg^{-1}, respectively, (c) comparison of the rate and capacity retention after 50 cycles of as-prepared MnO_2 NWs (in black), ZIF-67-MnO_2 NWs (in blue), C/Co (in green) and C/Co-MnO NWs (in pink) , and (d) comparison of the rate and capacity retention after 50 cycles of as-prepared C/Co-MnO NWs with other reported similar materials, such as C/nano-Si, [9] MOF-Derived porous Co_3O_4, [14] ZnO/Co_3O_4, [15] MnO@C, [17] MnO_2/MWCNT, [21] and Co-BDC MOF. [34]

and cyclic performance than that of controlled C/Co, MnO_2 NWs, ZIF-67-MnO_2 NWs and C/Co-MnO_2 physical mixture at the constant current density of 500, 1000, 2000 and 5000 mA g^{-1}, respectively, but also shows superior rate and cyclic performance than other reported similar materials, see Fig. 5d, such as C/nano-Si, [9] MOF-Derived porous Co_3O_4, [14] ZnO/Co_3O_4, [15] MnO@C, [17] MnO_2/MWCNT, [21] Co_3O_4/MnO_2 [32] and Co-BDC MOF. [34]

Furthermore, the as-prepared C/Co-MnO NWs also present much better rate capability than the controlled mixture C/Co-MnO_2 NWs, see Figs. 5, S4a and S4b. As shown in Figs. 1f, 3h, in-situ formed uniform carbon coating was fully covered on the surface of MnO NW, which has a strong interaction and created an integral electrical contact between MnO and carbon coating, similar mechanism could also be observed from that of the reported core–shell ZnO/$ZnFe_2O_4$@C mesoporous nanospheres. [35] However, There is only point electrical contact between the physically mixed MnO_2 NWs and the large size C/Co particles derived from ZIF-67, as present in Figs. S4a and S4b. Therefore, the synergistic effect of much improved conductivity and relatively suppressed volume change resulted from the integrally strong carbon coating should be responsible for the much superior rate and cyclic performance of C/Co-MnO NWs than that of the controlled mixture C/Co-MnO_2 NWs.

Conclusions

In this work, a novel and interesting structure of MOFs ZIF-67 on MnO_2 nanowire (NWs), like the candied hawthorn fruit on a stick, is designed and successfully prepared by using a controllable multi-step chemical method. The observed experimental results demonstrate that polyvinylpyrrolidone (PVP) modified surface is helpful for the growth of ZIF-67 on MnO_2 NWs and minimizing the MOF size from 500 to 100 nm. It is also interesting or exciting to find that the simultaneously formed carbon coating derived from ZIF-67 significantly promote the cyclic and rate performance of manganese oxide. Benefited from the synergistic effect of the highly conductive uniform carbon coating and the high capacity contribution from MnO, the finally obtained C/Co-MnO NWs deliver 848.4, 836.5, 834 and 718 $mAhg^{-1}$ at 500, 1000, 2000 and 5000 mAg^{-1} after 40 charge/discharge cycles, respectively. The achieved high rate and much enhanced cyclic performance make present C/Co-MnO NWs superior to other reported MOF-derived nanostructured materials.

Acknowledgements

This work was supported by National Natural Science Foundation of China (51402155), Priority Academic Program Development of Jiangsu Higher Education Institutions (PAPD) (YX03002), National Synergistic Innovation Center for Advanced Materials (SICAM), Foundation of NJUPT (NY214021).

References

1 B. Dunn, H. Kamath, J.M. Tarascon, Science, 2011, 334, 928. 2 A. Magasinski, P. Dixon, B. Hertzberg, A. Kvit, J. Ayala, G. Yushin, Nat. Mater., 2010, 9, 353.

3 L. Qie, W.M. Chen, Z.H. Wang, Q.G. Shao, X. Li, L.X. Yuan, X.L. Hu, W.X. Zhang, Y.H. Huang, Adv. Mater., 2012, 24, 2047.

4 Z.D. Huang, K. Zhang, T.T. Zhang, R.Q. Liu, X.J. Lin, Y. Li, T. Masese, X.M. Liu, X.M. Feng, Y.W. Ma, Energy Storage Mater., 2016, 5, 205.

5 Z.J. Li, D.B. Kong, G.M. Zhou, S.D. Wu, W. Lv, C. Luo, J.J. Shao, B.H. Li, F.Y. Kang, Q.H. Yang, Energy Storage Mater., 2017, 6, 98.

6 Y.L. Zhou, J. Tian, H.Y. Xu, J. Yang, Y.T. Qian, Energy Storage Mater., 2017, 6, 149.

7 Z.D. Huang, K. Zhang, T.T. Zhang, X.S. Yang, R.Q. Liu, Y. Li, X.J. Lin, X.M. Feng, Y.W. Ma, W. Huang, Energy Storage Mater., 2016, 3, 36.

8 Z.D. Huang, K. Zhang, T.T. Zhang, R.Q. Liu, X.J. Lin, Y. Li, X.M. Feng, Q.B. Mei, T. Masese, Y.W. Ma, W. Huang, Composites Part A: Applied Science and Manufacturing, 2016, 84, 386.

9 Y.H. Song, L. Zuo, S.H. Chen, J.F. Wu, H.Q. Hou, L. Wang, Electrochim. Acta, 2015, 173, 588.

10 Y.Z. Han, P.F. Qi, X. Feng, S.W. Li, X.T. Fu, H.W. Li, Y.F. Chen, J.W. Zhou, X.G. Li, B. Wang, ACS Appl. Mater. Interfaces, 2015, 7, 2178.

11 B. Liu, X.B. Zhang, H. Shioyama, T. Mukai, T. Sakai, Q. Xu, J. Power Sources, 2010, 195, 857.

12 C. Li, T.Q. Chen, W.J. Xu, X.B. Lou, L.K. Pan, Q. Chen, B.W. Hu, J. Mater. Chem. A, 2015, 3, 5585.

13 G. Huang, F.F. Zhang, X.C. Du, Y.L. Qin, D.M. Yin, L.M. Wang, ACS Nano, 2015, 9, 1592.

14 D. Tian, X.L. Zhou, Y.H. Zhang, Z. Zhou, X.H. Bu, Inorg. Chem., 2015, 54, 8159.

15 D.Q. Zhu, F.C. Zheng, S.H. Xu, Y.G. Zhang, Q.W. Chen, Dalton Trans., 2015, 44, 16946.

16 F. Cheng, W.C. Li, A.H. Lu, ACS Appl. Mater. Interfaces, 2016, 8, 27843.

17 F.C. Zheng, G.L. Xia, Y. Yang Q.W. Chen, Nanoscale, 2015, 7, 9637.

18 Y.H. Wang, X. Ding, F. Wang, J.Q. Li, S.Y. Song, H.J. Zhang, Chem. Sci., 2016, 7, 4284.

19 J.G. Wang, D.D. Jin, R. Zhou, X. Li, X.R. Liu, C. Shen, K.Y. Xie, B.H. Li, F.Y. Kang, B.Q. Wei, ACS Nano, 2016, 10, 6227.

20 F.C. Zheng, D.Q. Zhu, X.H. Shi, Q.W. Chen, J. Mater. Chem. A, 2015, 3, 2815.

21 S.J. Ee, H.C. Pang, U. Mani, Q.Y. Yan, S.L. Ting, P. Chen, ChemPhysChem, 2014, 15, 2445.

22 S.Z. Huang, Q. Zhang, W.B. Yu, X.Y. Yang, C. Wang, Y. Li, B.L. Su, Electrochim. Acta, 2016, 222, 561.

23 S.Z. Huang, Y. Cai, J. Jin, J. Liu, Y. Li, Y. Yu, H.E. Wang, L.H. Chen, B.L. Su, Nano Energy, 2015, 12, 833.

24 S.Z. Huang, J. Jin, Y. Cai, Y. Li, Z. Deng, J.Y. Zeng, J. Liu, C. Wang, T. Hasan, B.L. Su, Scientific Reports, 2015, 5, 14686.

25 S.Z. Huang, J. Jin, Y. Cai, Y. Li, Y.H. Tan, E. B. Wang, G. Tendeloo, B.L. Su, Nanoscale, 2014, 6, 6819.

26 Y. Xia, B.B. Wang, G. Wang, XX.J. Liu, H. Wang, ChemElectroChem, 2016, 3, 299.

27 P.Y. Wang, J.W. Lang, D.X. Liu, X.B. Yan, Chem. Commun., 2015, 51, 11370.

28 W. Yin, D. Yuei, X.G. Liu, S.B. Sun, J.P. Cao, X. Ma, C.H. Zhang, J.Y. Kang, Li.W. Lin, ACS Appl. Mater. Interfaces, 2016, 8, 3992.

29 Z.L. Xiu, D.Y. Kim, M. H. Alfaruqi, J.H. Gim, J.J. Song, S.J. Kim, P.T. Duong, J.P. Baboo, V. Mathew, J. Kim, J. Mater. Chem. A, 2016, 4, 4706.

30 M. Ramesh, H.S. Nagaraja, M.P. Rao, S. Anandan, N.M. Huang, Mater. Lett., 2016, 172, 85.

31 Q.F. Wang, R.Q. Zou, W. Xia, J. Ma, B. Qiu, A. Mahmood, R. Zhao, Y. Yang, D.G. Xia, Q. Xu, Small, 2015, 11, 2511.
32 Q. Zhu, Y.H. Li, Y. Gao, Chem. Eur. J.,2016, 22, 6876.
33 S.Z. Huang, Q. Zhang, W.B. Yu, X.Y. Yang, C. Wang, Y. Li, B.L. Su, Electrochim. Acta, 2016, 222, 561.
34 X.S. Hu, H.P. Hu, C. Li, T. Li, X.B. Lou, Q. Chen, B.W. Hu, J. Solid State Chem., 2016, 242, 71.
35 C.Z. Yuan, H. Cao, S.Q. Zhu, H. Hua and L.R. Hou, J. Mater. Chem. A 2015, 3, 20389.

Supplementary information

High Rate Li-Ion Storage Property of MOFs-Carbonized Derivatives Coating on MnO Nanowires

Zhen-Dong Huang [a], [†] *Zhen Gong* [a], [†] *Qi Kang* [a], *Yanwu Fang* [a], *Xu-Sheng Yang* [b], *Ruiqing Liu* [a], *Xiujing Lin* [a], *Xiaomiao Feng* [a], *Yanwen Ma* [a],* *and Dan Wang* [a, c],*

[a] Key Laboratory for Organic Electronics and Information Displays & Institute of Advanced Materials (IAM), Jiangsu National Synergetic Innovation Center for Advanced Materials (SICAM), Nanjing University of Posts & Telecommunications, Nanjing 210023, China.

[b] Advanced Manufacturing Technology Research Centre, Department of Industrial and Systems Engineering, The Hong Kong Polytechnic University, Hung Hom, Kowloon, Hong Kong, China.

[c] State Key Laboratory of Multiphase Complex Systems Institute of Process Engineering Chinese Academy of Sciences, No. 1, Beiertiao, Zhongguancun, Beijing, 100190, P.R. China.

[†] *Dr. Huang and Mr. Gong have the equal contribution to this paper.*

* Corresponding authors:

iamywma@njupt.edu.cn (Y.W. Ma); danwang@mail.ipe.ac.cn (D Wang).

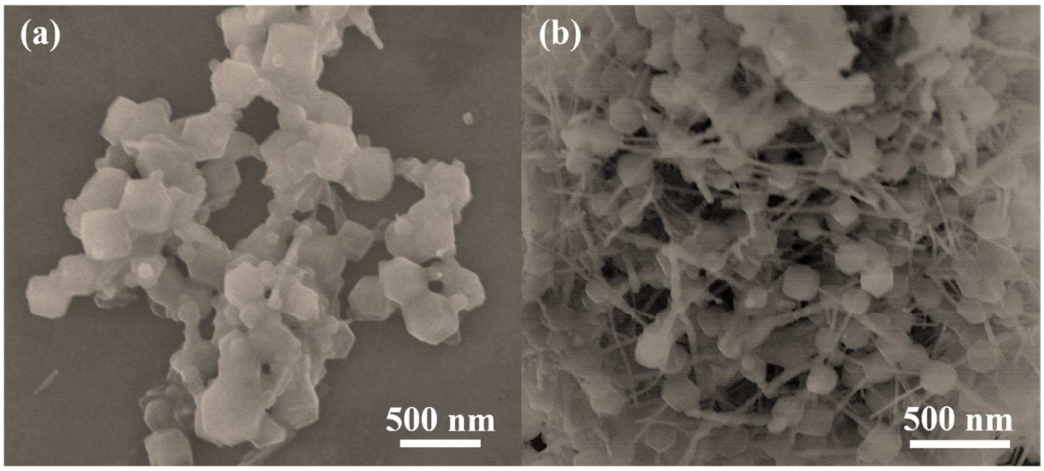

Fig. S1. Scanning electron microscopy (SEM) images of as-prepared ZIF-67-MnO_2 NWs mixture without using PVP (a) and the derivative of ZIF-67-MnO_2 NWs heat-treated at 300 ^{o}C for 2 h (b).

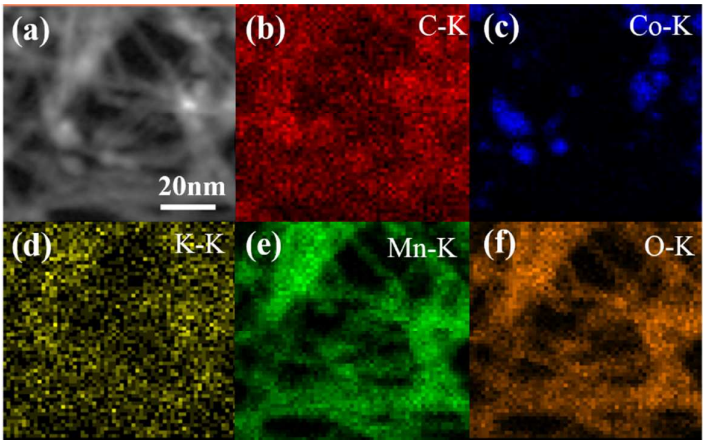

Fig. S2. Acquire HAADF TEM images of carbonized derivative of ZIF-67-MnO_2 NWs (C/Co-MnO NWs) (a), and the corresponding element mapping of C (b), Co (c), K (d), Mn (e) and O (f), respectively.

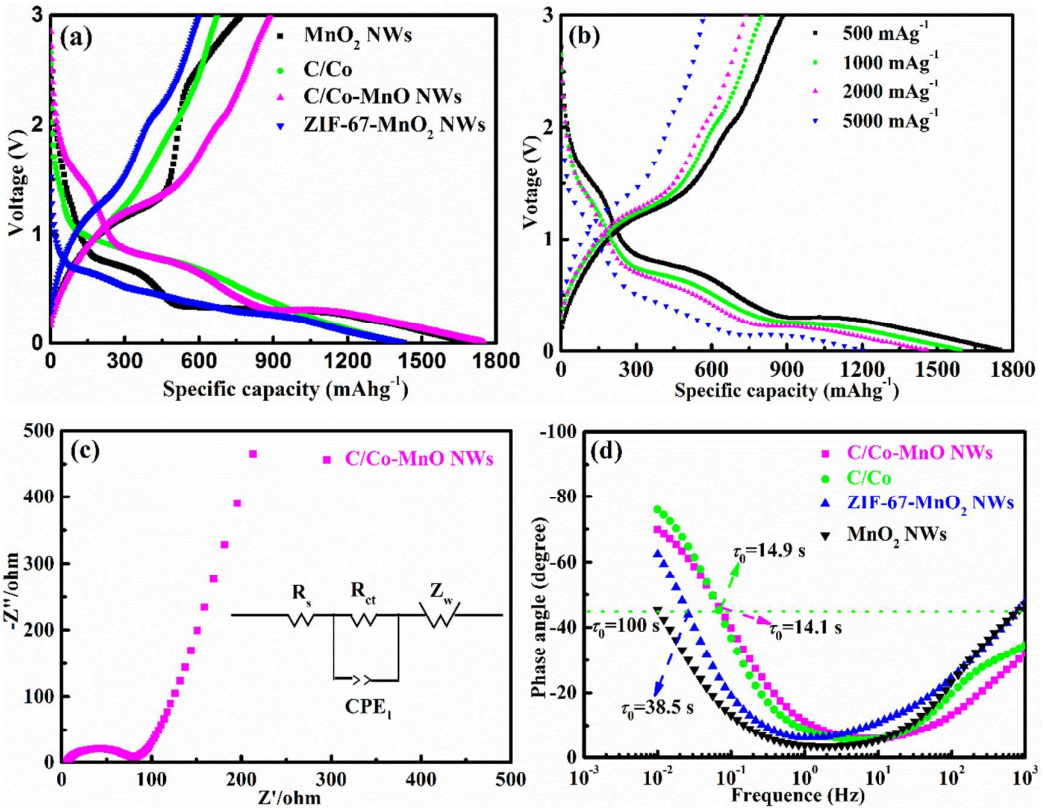

Fig. S3. The first cycle charge/discharge profiles corresponding to (a) the as-prepared MnO_2 NWs, C/Co, C/Co-MnO NWs and ZIF-67-MnO_2 NWs and (b) C/Co-MnO NWs at the current density ranged from 500 to 5000 mAg^{-1}, respectively, (c) The electrochemical impedance spectra of the C/Co-MnO NWs, (d) the Bode plots of C/Co-MnO NWs, C/Co, ZIF-67-MnO_2 NWs, and MnO_2 NWs, respectively.

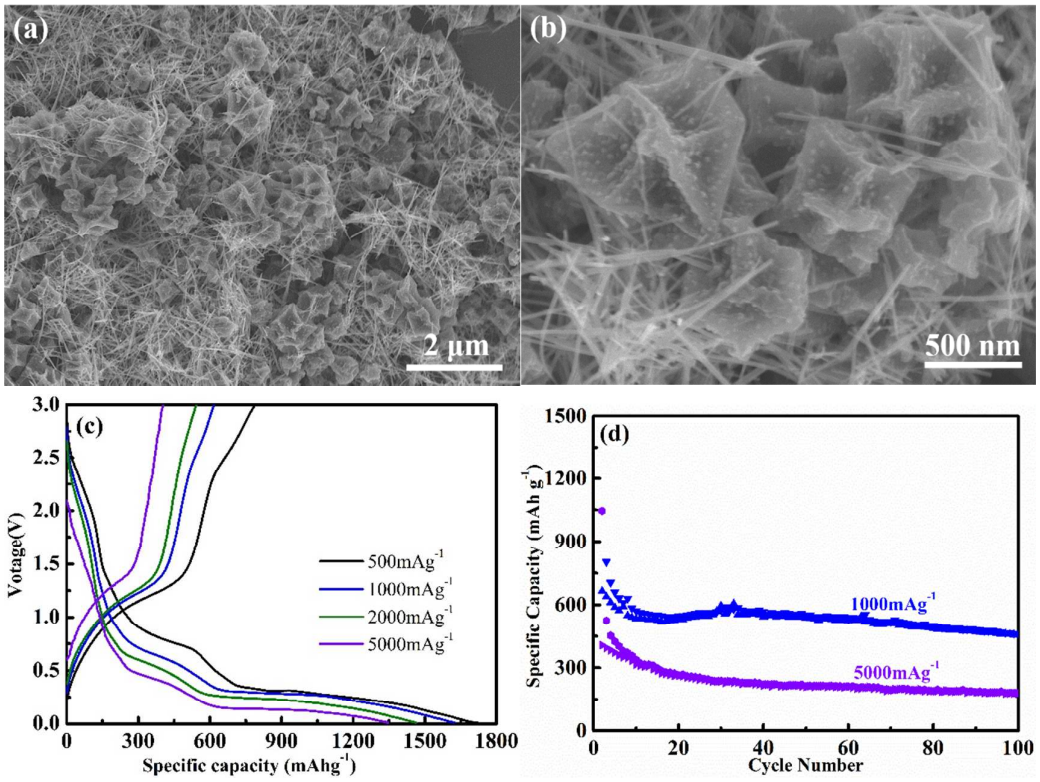

Fig. S4. (a) and (b) The SEM images, (c) the first cycle charge/discharge profiles and (d) the cyclic performance at different current density of the controlled physical mixture of MnO_2 NWs and Co/C derivatives. The mixtures was prepared by physically mixing the as-prepared MnO_2 NWs (75*wt*%) and Carbonized ZIF-67 (25*wt*%) via ultrasonication in ethanol, followed by drying the dispersion at 60 ^{o}C for 10 h in blowing drying oven.

Table of Contents Graphic and Synopsis

The carbonized derivatives of MOFs ZIF-67 on MnO_2 NWs are fabricated as high rate Li-ion storage anode materials.